Production of p-Type Si/n-Type β-$FeSi_2$ Heterojunctions Using Facing-Targets Direct-Current Sputtering and Evaluation of Their Resistance and Interface State Density

Rawiwan Chaleawpong, Nathaporn Promros, Peerasil Charoenyuenyao, Adison Nopparuchikun, Phongsaphak Sittimart, Tomohiro Nogami, and Tsuyoshi Yoshitake*

Without a post-annealing procedure, the β-$FeSi_2$ thin films are epitaxially grown on Si(111) wafer substrates via facing-targets direct-current sputtering. During epitaxial growth, the temperature for heating of substrates is maintained at 600 °C. The resultant p-type Si/n-type β-$FeSi_2$ heterojunctions are produced. At room temperature, a large leakage current under an applied reverse bias voltage together with a small photo-detective performance is observed from the measured dark and irradiated current density–voltage curves of the created heterojunctions. Both of the conductance–voltage (G/ω–V) and capacitance–voltage (C–V) measurements at different frequencies (f) in the range of 5 kHz–1 MHz are performed in the dark at room temperature. The interface state density (N_{ss}) and series resistance (R_s) in the created p-type Si/n-type β-$FeSi_2$ heterojunctions are computed and analyzed from the measured C–V–f and G/ω–V–f curves. N_{ss} is found to be 3.48×10^{12} eV^{-1} cm^{-2} at 5 kHz and decreased to 4.68×10^{11} eV^{-1} cm^{-2} at 1 MHz. Moreover, the values of R_s at zero bias are 2.21 kΩ at 5 kHz and 13.66 Ω at 1 MHz. These results review the presence of N_{ss} and R_s in the created heterojunctions, and they can be the cause to degrade the heterojunction performance.

1. Introduction

In recent years, many research groups have studied and demonstrated that the orthorhombic semiconducting phase (β) for iron disilicide ($FeSi_2$) could be epitaxially created on Si with lattice mismatches of 2–5 percent. This has received considerable attention because of its many desirable semiconducting properties.[1–3] It was evidently affirmed in previous research that β-$FeSi_2$ owned an absorption coefficient greater than 10^5 cm^{-1} at a photon energy of 1.2 eV[4,5] and an indirect optical band gap of 0.76 eV below a direct optical band gap of 0.85 eV.[6,7] These optical band gaps corresponded to the wavelengths of optical fiber telecommunications in the range between 1.3 and 1.55 μm. It is well known that this is composed from eco-friendly elements of Fe and Si. Both Fe and Si are non-toxic and exist as natural resources in abundance.[8,9] These features of β-$FeSi_2$ are appropriate for utilization in applications of low-cost optoelectronic devices.

For achieving β-$FeSi_2$ thin films with considerable quality, many techniques for film creation have been previously utilized to produce β-$FeSi_2$ thin films including ion beam synthesis,[10] molecular beam epitaxy,[11,12] and reactive deposition epitaxy.[13,14] All of these approaches needed to employ post-annealing at high temperatures of around 800 °C. It was previously reported that post-annealing at high temperatures was the main reason for the Fe atom diffusion from the side of the β-$FeSi_2$ films into the side of the Si wafer.[15–19] The diffused Fe atoms could create deep trap levels in the depletion region. This formed a trap center for the minority carrier as well as increased the leakage current of the heterojunctions, which led to the degradation of the photo-detective performance for the created heterojunctions.[20,21] For this reason, the creation of β-$FeSi_2$ thin films should be performed at a low substrate temperature.

We previously employed facing-targets direct-current sputtering (FTDCS) for the low-temperature growth of β-$FeSi_2$. When compared to the conventional sputtering method, FTDCS has the following advantages: a) low-pressure sputtering owing to

R. Chaleawpong, Dr. N. Promros, P. Charoenyuenyao, A. Nopparuchikun, P. Sittimart
Department of Physics
Faculty of Science
King Mongkut's Institute of Technology Ladkrabang
1 Soi Chalongkrung 1, Ladkrabang, Bangkok 10520, Thailand
E-mail: popphy11037@gmail.com

T. Nogami, Prof. T. Yoshitake
Department of Applied Science for Electronics and Materials
Kyushu University
6-1 Kasuga, Fukuoka 816-8580, Japan

DOI: 10.1002/pssa.201701022

plasma species being effectively confined by electric and magnetic fields between the facing targets; b) damage to substrate surfaces is low since the substrates are free of plasma; c) a small increase in the substrate temperature.[5,19,20,22] Additionally, species arriving at the substrate surface have higher kinetic energy than those in other methods, such as molecular beam epitaxy, due to low-pressure sputtering.[19,20] There has been previous success in the epitaxial creation of β-$FeSi_2$ thin films onto Si(111) wafers via FTDCS, at a temperature for substrate heating of 600 °C.[20] This temperature for substrate heating is below the substrate temperature at which epitaxial creation is achieved by the utilization of post-annealing. The β-$FeSi_2$ thin films that were epitaxially created on the Si(111) wafer presented n-type conduction together and the carrier densities of a p-type Si substrate and β-$FeSi_2$ films at 300 K are approximately $1.5 \times 10^{15}\,cm^{-3}$ and $1.0 \times 10^{17}\,cm^{-3}$, respectively.[5,20] The β-$FeSi_2$ films have an electrical conductivity of approximately $23\,S\,cm^{-1}$ at 300 K. Therefore, the resistivity of β-$FeSi_2$ films is around $4.3 \times 10^{-2}\,\Omega$ cm.[20]

The detection of near-infrared (NIR) light for the created p-type Si/n-type β-$FeSi_2$ heterojunctions was studied.[5,18,21,23] However, these heterojunctions demonstrated a small photodetective performance leading to small values of the photovoltaic and photodiode properties. This result was possible due to the interface states existing at the heterojunction interface in addition to the Fe atom diffusion from the side of the β-$FeSi_2$ film into the side of the Si wafer.[15–19,24] These caused a trap center of the photo-generated carrier and the source of leakage current.[16–19,24] However, calculation of the existing series resistance (R_s) and interface state density (N_{ss}) for the p-type Si/n-type β-$FeSi_2$ heterojunctions produced via FTDCS has never been studied.

In this present study, the researchers estimated N_{ss} as well as R_s of the p-type Si/n-type β-$FeSi_2$ heterojunctions created by the employment of FTDCS and studied their characteristics at different frequencies (f) from the extraction of the measured conductance–voltage–frequency (G/ω–V–f) and capacitance–voltage–frequency (C–V–f) in the dark. N_{ss} and R_s were computed by means of the Hill-Coleman and Nicollian-Brews approaches. According to the available information, this was the first study and report on N_{ss} and R_s estimations at different f for the p-type Si/n-type β-$FeSi_2$ heterojunctions created by the utilization of FTDCS.

2. Experimental Section

By utilization of FTDCS, an n-type β-$FeSi_2$ layer, which had a film thickness of 300 nm, was epitaxially created onto a p-type Si(111) wafer at a substrate temperature of 600 °C employing a pair of $FeSi_2$ alloy targets. Before the epitaxial creation, the researchers used two solvents to rinse the organic residues and oils on the surface of the Si wafer. Initially, they used acetone to rinse the Si wafer. Next, the acetone was rinsed by methanol and deionized water in sequence. The period for the rinsing of each step was 5 min. For removing the native oxide layer that existed on the Si wafer surface, the Si wafer was dipped in a hydrofluoric acid (HF) solution. Next, it was removed and cleaned in deionized water. After that, the cleaned Si wafer was mounted on a substrate holder inside a chamber of FTDCS. The inside of this chamber was vacuumed at a base pressure of around 3×10^{-5} Pa by utilizing a turbomolecular pump, which was connected to a rotary pump. The $FeSi_2$ targets and substrates were separated by a space of 75 mm. Ar gas (purity: 6N) was fed into the inside of the FTDCS chamber at a constant flow rate of 15 sccm during the sputtering. After that, the sputtering pressure was adjusted and fixed at 1.33×10^{-1} Pa. The applied V was adjusted to be 1 kV and the generated discharge current was 1.5 mA. After the epitaxial creation of the β-$FeSi_2$ films on the Si wafer, the sample was moved to the radio-frequency magnetron sputtering (RFMS) system for the formation of the back and front metallic electrodes. In order to form the front Ohmic contact in a finger-shaped pattern onto the Si wafer surface, palladium (Pd) films were coated by using a metal mask having a finger-shaped pattern at room temperature. To form the back Ohmic contact in a rectangular shape on the whole surface of the β-$FeSi_2$ films, aluminium (Al) films were coated by using a metal mask having a rectangular shape at room temperature. Prior to the creation of electrodes, the prepared heterojunctions were dipped with a 1% HF solution and rinsed with deionized water to remove the natural oxide layer. The creation of the electrodes was carried out under the conditions shown in **Table 1**. **Figure 1** presents a schematic diagram of the created heterojunctions including both the Pd and Al electrodes. Pd and Al electrodes were coated at room temperature to form Ohmic contact. The Pd/Si and Al/β-$FeSi_2$ Ohmic contacts were confirmed from the measurements of current–voltage (I–V) characteristics. These measurements were performed between the isolated electrodes on the same surface side. The measured I–V characteristics of Pd/Si and Al/β-$FeSi_2$ Ohmic contacts are shown in **Figure 2**a and b, respectively.

The study of the surface morphology of the films created by FTDCS was operated with a Carl Zeiss Auriga Field Emission Scanning Electron Microscope (FESEM). The cross section of the films was investigated by the utilization of FESEM (Hitachi S-4700 Scanning Electron Microscope). The crystalline structure was examined by employment of X-ray diffraction (XRD) (Rigaku RINT 2000/PC). The measurements of I–V characteristics under reverse and forward bias conditions were performed by utilizing a Keithley 2400 source meter in the dark and under illumination with a 6-mW, 1.31-μm laser light (Neoark, TC20). The measurements of the G/ω–V and C–V characteristics of the

Table 1. Conditions for creation of Al and Pd Ohmic contacts via RFMS.

	Al Ohmic contact	Pd Ohmic contact
Sputtering target	Al (purity: 4N)	Pd (purity: 4N)
Base pressure	1×10^{-5} Pa	1×10^{-5} Pa
Substrate temperature	Room temperature	Room temperature
Operating pressure	2.66×10^{-1} Pa	1.33×10^{-1} Pa
Flow rate of Ar gas	10 sccm	10 sccm
Sputtering power	200 W	200 W
Deposition rate	4.2 nm min^{-1}	8.3 nm min^{-1}
Thickness of film	500 nm	500 nm

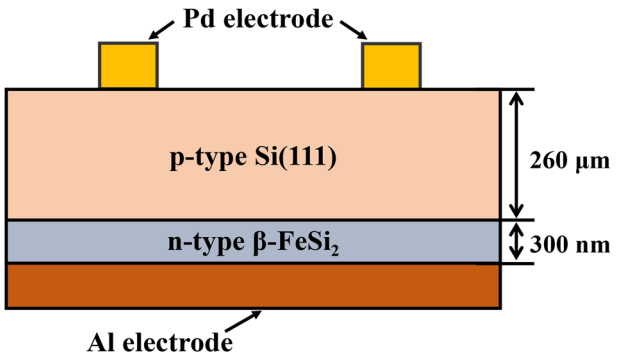

Figure 1. A schematic diagram of the p-type Si/n-type β-$FeSi_2$ heterojunctions created by the utilization of FTDCS.

heterojunctions were carried out in f range from 5 kHz to 1 MHz by utilizing an Agilent E4980A Precision LCR Meter. From the measured C–V–f and G/ω–V–f curves, R_s and N_{ss} were extracted by means of the Nicollian-Brews and Hill-Coleman approaches, respectively.

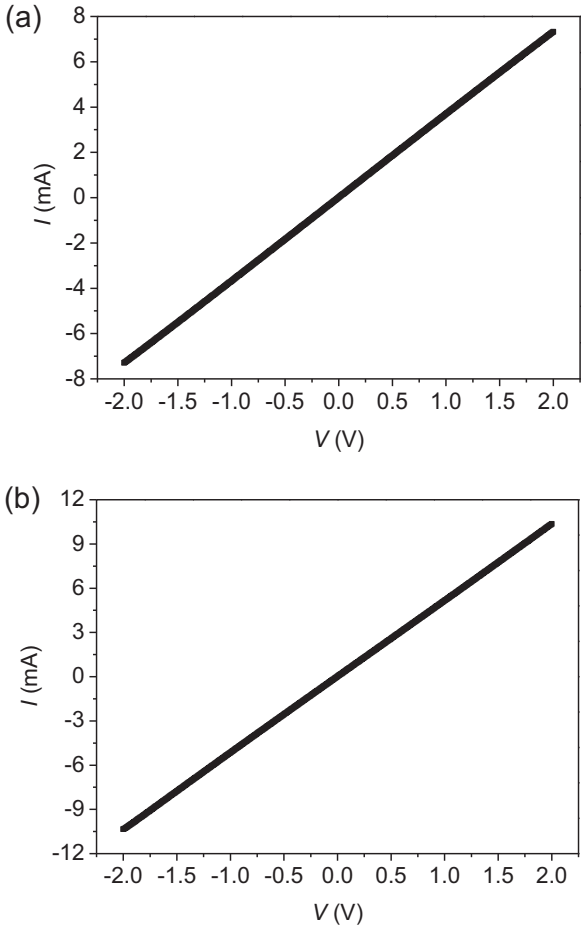

Figure 2. The measured I–V characteristics for (a) the Pd/Si and (b) Al/β-$FeSi_2$ Ohmic contacts.

3. Results and Discussion

Figure 3a shows the FESEM image in plain view of the β-$FeSi_2$ thin film. It can be seen that the film comprised a large number of crystallites with the small size covering the film's surface. Moreover, the created films contained many grain boundaries. Thus, the photogenerated carriers should be trapped by the grain boundaries, which resulted in the degradation of the light detection properties. Figure 3b presents an FESEM image in the cross section of the β-$FeSi_2$ films created on Si wafer substrates. The β-$FeSi_2$ films created by FTDCS were uniform and free of cracks. Additionally, a sharp interface can be seen between the Si wafer substrates and the β-$FeSi_2$ films.

Figure 4 depicts the XRD pattern of the created β-$FeSi_2$ thin films on Si(111) wafers, which was measured in a 2θ–θ scan. Weak 404/440 and intense 202/220 peaks from the 2θ–θ XRD pattern were found. Both peaks are the typical XRD peaks of the β-$FeSi_2$ thin films epitaxially created on Si(111). The inset in Figure 4 shows the XRD pattern in a 2θ scan with an incidence angle of 4°. The 2θ XRD pattern showed no peaks. Namely, no β phase diffraction peaks appeared in 2θ-scan, indicating that the β-$FeSi_2$ films were epitaxially grown on Si(111) substrates without polycrystalline structure.[5,18] On the other hand, the β-$FeSi_2$ films will include the polycrystalline structure if the 2θ pattern exhibits several β phase diffraction peaks of β-$FeSi_2$.[25,26]

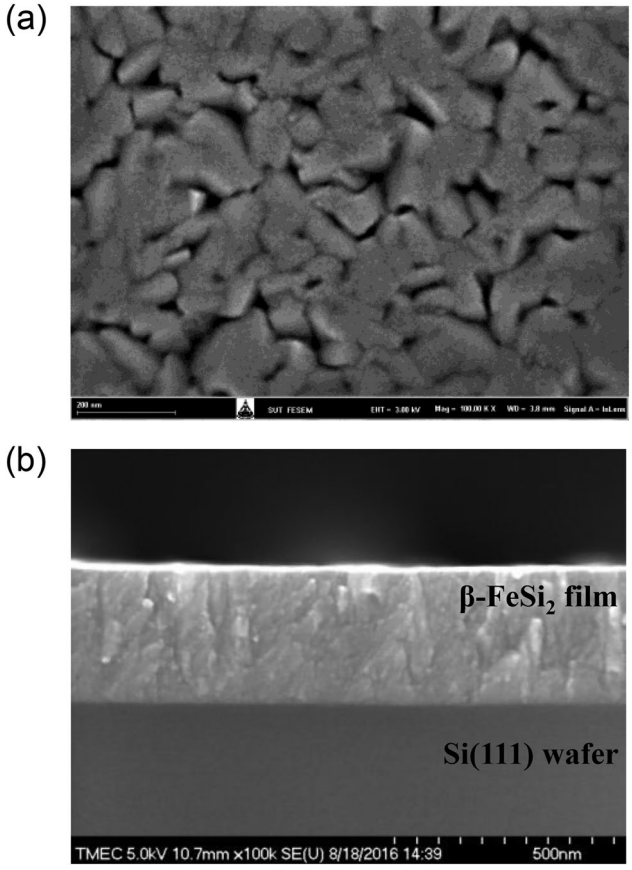

Figure 3. FESEM images (a) in plain view and (b) cross section of the β-$FeSi_2$ films created by the utilization of FTDCS.

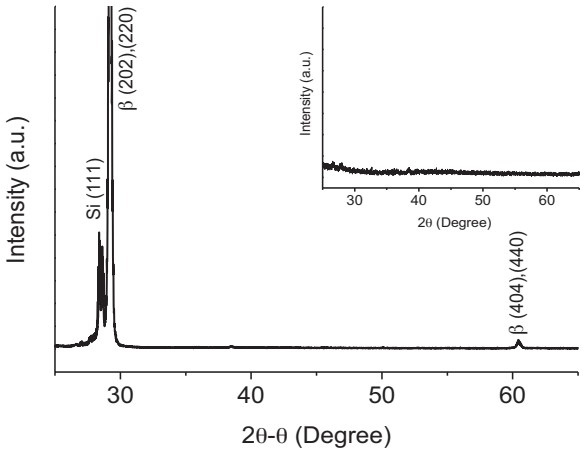

Figure 4. The XRD pattern of a β-$FeSi_2$ thin film created onto the Si(111) wafer, which was measured in a 2θ–θ scan. The inset of this figure demonstrates the XRD pattern measured in a 2θ scan with an incidence angle of 4°.

The pattern of the pole figure for the diffraction peak of the β-440/404 of the β-$FeSi_2$ films created on the Si(111) wafers is illustrated in **Figure 5**. This indicates the presence of three types of epitaxial variants rotated at an angle of 120° with respect to each other.

The room temperature current density–voltage (*J*–*V*) curves for the p-type Si/n-type β-$FeSi_2$ heterojunctions, which were measured under applied reverse and forward *V* in the dark and under illumination with a 6-mW, 1.31-μm laser, are presented in **Figure 6**. It was clear that the created p-type Si/n-type β-$FeSi_2$ heterojunctions demonstrated a good rectifying action similar to the common p-n junction. The ratio between the forward dark and reverse dark currents at *V* of ±1 V was higher than the two orders of magnitude. In addition, a large leakage current was observed as well as a small response from irradiation by NIR light under reverse *V* conditions. These should be possible for the interface states existing at the hetero-interface in addition to the Fe atoms that diffused from the side of the β-$FeSi_2$ films to the side of the Si wafer during the film creation.[15–19,24] These behave as the source of leakage current and a trap center of the photo-generated carrier.[16–19,24] The inset of Figure 6 presents the plot of the photocurrent subtracted from the dark current versus *V*. The subtracted current increased from 2.0×10^{-5} A cm^{-2} at 0 V, and it reached a maximum value of 3.9×10^{-5} A cm^{-2} at −3 V.

Figure 7a and b show *f* dependence of *C*–*V* and *G*/*ω*–*V* curves of p-type Si/n-type β-$FeSi_2$ heterojunctions, which were measured under *f* range of 5 kHz to 1 MHz at room temperature. In *V* range of −5 to 5 V, both *C*–*V*–*f* and *G*/*ω*–*V*–*f* plots exhibit three regimes (inversion, depletion, and accumulation regions).[27] *C* is increased with the increment of *V* until it reaches into an accumulation region.[28–32] At higher *V*, strong accumulation in our case is around 5 V.[29,30,33,34] The values of *C* and *G*/*ω* are dependent on both *V* and *f*. The changes in *C* and *G*/*ω* occur particularly in the depletion and accumulation regions, while they remain almost constant in the inversion region.[27] *C* increases with increasing positive *V* until it reaches an accumulation steady state. We observed a rise in *C* for lower *f* values. At low *f* values, *C* corresponds to the sum of the interface and space charge capacitance. As *f* increases, the contribution of the interface *C* to the device *C* decreases.[27] The presence of *C* peak in the *C*–*V* plot is likely due to the molecular restructuring and reordering of N_{ss} and R_s.[30] The peak position shifts to lower *V* values by decreasing *f* value. The peak intensity of each *C*–*V* curve decreases when *f* value is rose. Also, the peak intensity of the *G*/*ω*–*V* characteristics decreases with increasing *f*. This indicates that the interface states can follow an alternative current (AC) signal.[35] The peak position shifts to higher positive *V* values with increasing *f*.

In order to extract R_s of the heterojunction diode in the current estimation, we utilized the method of Nicollian and Goetzberger.[36,37] *f* dependent *C*–*V* and *G*/*ω*–*V* characteristics of heterojunctions were measured in *f* range of 5 kHz–1 MHz. At sufficiently high *f* value, the diodes are biased into strong accumulation to determine R_s.

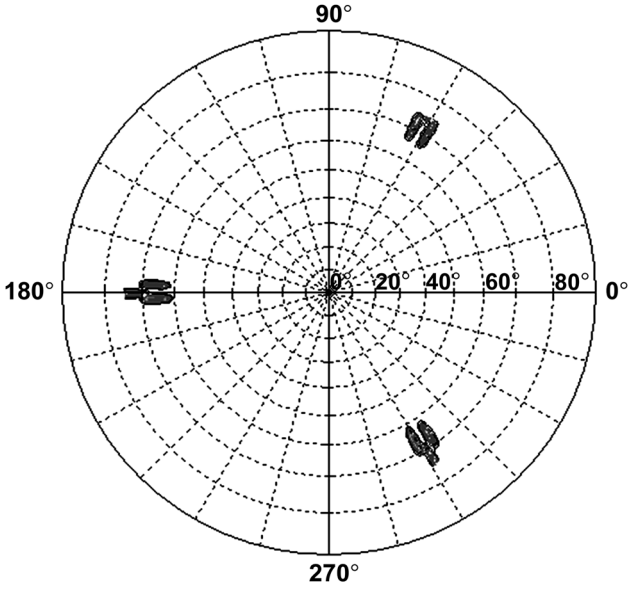

Figure 5. The XRD pole figure pattern for the diffraction peak of β-440/404 of the β-$FeSi_2$ films created by the employment of FTDCS.

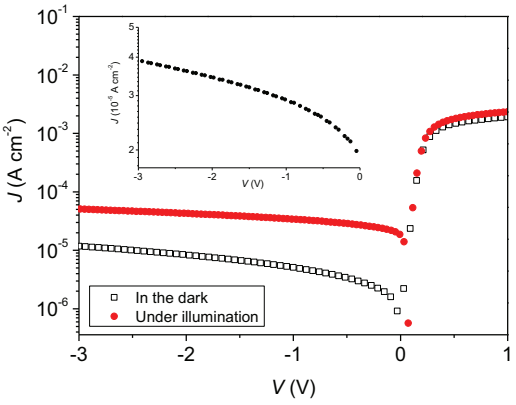

Figure 6. The room temperature *J*–*V* curves of the junctions measured in the dark and under illumination. The inset of this figure depicts the illumination current subtracted from the dark current.

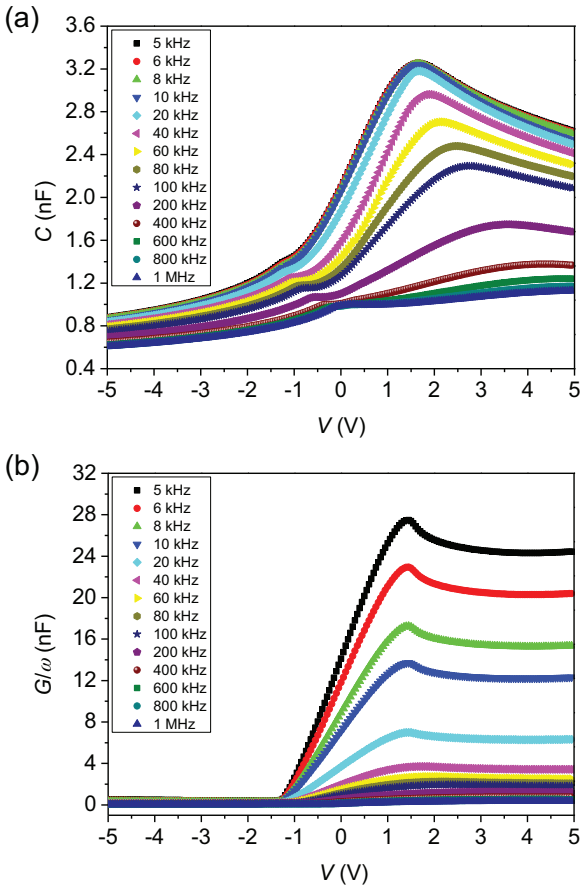

Figure 7. a) The values of f dependence of C–V and b) G/ω–V curves of p-type Si/n-type β-$FeSi_2$ heterojunctions.

Then, the admittance (Y_{ma}) in terms of capacitance (C_{ma}) and equivalent parallel conductance (G_{ma}) is given by:[32]

$$Y_{ma} = G_{ma} + j\omega C_{ma} \tag{1}$$

where R_s is the real part of the impedance ($Z_{ma} = 1/Y_{ma}$). Thus, R_s of devices can be subtracted from the measured C_{ma} and G_{ma} in strong accumulation at high f.[36,38,39] Comparing the real and imaginary parts of the impedance from C–V and G/ω–V measurements in strong accumulation, R_s was calculated by the relationship:

$$R_s = \frac{G_{ma}}{(C_{ma}\omega)^2 + G_{ma}^2} \tag{2}$$

where ω is the angular frequency, G_{ma} and C_{ma} are the values of conductance and capacitance obtained in the strong accumulation region, respectively.

The capacitance of the insulator layer (C_{ox}) is obtained by substituting R_s into the relation:

$$C_{ma} = \frac{C_{ox}}{1 + \omega^2 R_s^2 C_{ox}^2} \tag{3}$$

From C–V and G/ω–V measurements in the accumulation region, C_{ox} was calculated by the relationship:

$$C_{ox} = C_{ma}\left(\frac{G_{ma}^2}{C_{ma}^2\omega^2} + 1\right) \tag{4}$$

The relation of R_s as a function of V at different f for the heterojunctions is shown in **Figure 8**. The obtained values for R_s in Figure 8 were computed from Equation (2). As seen in Figure 8, the values of R_s are nearly constant in the inversion and accumulation regions. R_s gives a peak at low f values (≤100 kHz) in the depletion region (V range about −1 V to 1 V) and almost disappears at sufficiently high f values (>100 kHz). With increasing f value, the magnitude of the peak decreases. This can be explained by the fact that interface states become effective at low f values.[32,35,40] The peak position shifts to forward V with increasing f value. This might be attributed to a special density distribution of N_{ss} at p-type Si/n-type β-$FeSi_2$ heterojunctions, including reordering and restructuring under applied bias effect at different f values.[32,35,40] V-dependent R_s values remain almost constant at high f values (>100 kHz). This indicates that the interface charges have enough energy to escape from the trap levels.[41] Also, the charges at the interface states could not follow the AC signal at high f values.[39] The plot of R_s–f for the p-type Si/n-type β-$FeSi_2$ heterojunctions, at zero bias V, has been provided as shown in **Figure 9**. From Figure 9, the values of R_s at 0 V were 2.21 kΩ at 5 kHz and 13.66 Ω at 1 MHz. The presence of R_s in the p-type Si/n-type β-$FeSi_2$ heterojunctions could be due to the diffused Fe atoms on the side of the Si wafer during creation.[23,24] This diffusion would form deep trap levels in the depletion region and produce the leakage of the current.[18,23,24] Furthermore, light detection was inhibited since the photo-generated carriers were trapped in the deep-trap levels.[18,23,24]

The estimation of N_{ss} in the p-type Si/n-type β-$FeSi_2$ heterojunctions is very important because the existence of N_{ss} is the main cause for impairment of the device's performance. The value of f dependence of N_{ss} can be obtained from the C–V and G/ω–V measurements by utilizing the Hill-Coleman method. Based on this method, N_{ss} is given by:[41–46]

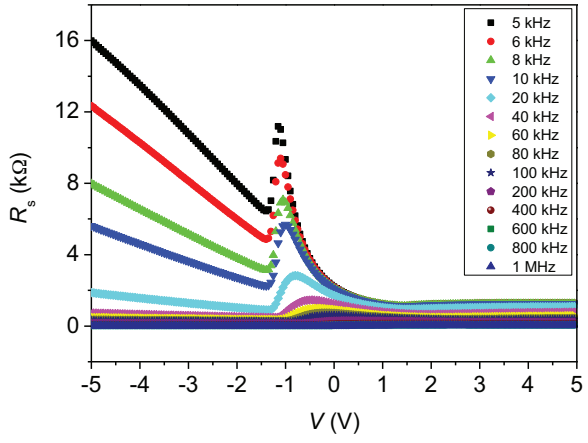

Figure 8. The variation of R_s as a function of V at different f for the heterojunctions.

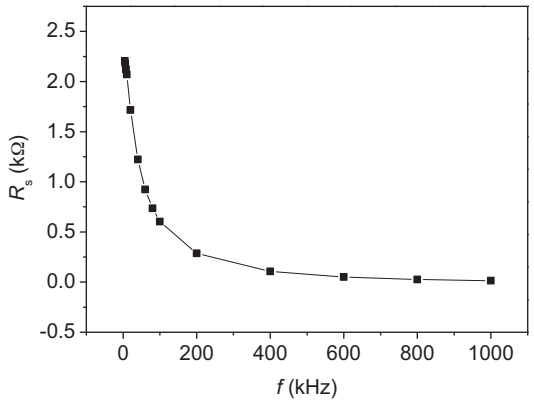

Figure 9. Relationship between R_s and f at zero bias for p-type Si/n-type β-$FeSi_2$ heterojunctions.

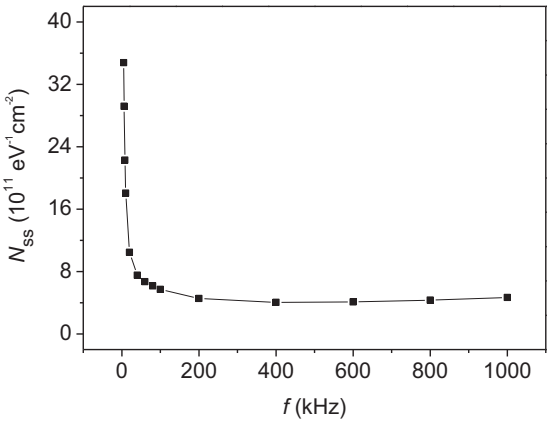

Figure 10. The values of N_{ss} for p-type Si/n-type β-$FeSi_2$ heterojunctions as a function of f at room temperature.

$$N_{ss} = \frac{2}{qA}\left(\frac{(G_m/\omega)_{max}}{(1 - C_m/C_{ox})^2 + ((G_m/\omega)_{max}/C_{ox})^2}\right) \quad (5)$$

where ω is the angular frequency and A is the junction area (0.1 cm^2), $(G_m/\omega)_{max}$ is the maximum measured conductance value and C_m is C corresponding to $(G_m/\omega)_{max}$.[41–43,45,47] C_{ox} is the capacitance of the insulator layer. In this case, we assumed that there was a thin intrinsic layer of β-$FeSi_2$ existing between p-type Si and n-type β-$FeSi_2$. Namely, the insulator layer means a thin intrinsic layer of β-$FeSi_2$. C_{ox} is the capacitance of the thin intrinsic layer of β-$FeSi_2$. C_{ox} can be obtained from the measured G/ω–V–f and C–V–f in strong accumulated regions through utilization of Equation (4).[41,48–50]

The values of various parameters for p-type Si/n-type β-$FeSi_2$ heterojunctions determined from C–V and G/ω–V characteristics in f range of 5 kHz–1 MHz are given in **Table 2**. **Figure 10** presents the variation of N_{ss} for the p-type Si/n-type β-$FeSi_2$ heterojunctions as a function of f at room temperature. N_{ss}, which was estimated by Equation (5), increased exponentially with decreasing f value. As clearly observed in Figure 9, the estimated N_{ss} in the low f region (≤100 kHz) depended on f, causing the increment of C in the p-type Si/n-type β-$FeSi_2$ heterojunctions. At high f values (above 100 kHz), N_{ss} was independent of f. The high C values at low f values were attributed to the excess C resulting from N_{ss}, which is in equilibrium with the semiconductor that follows the AC signal.[31,41,48,50] In contrast, the interface states in equilibrium with the semiconductor do not contribute to C at adequate f. Also, the charge at the interface states cannot follow the AC signal.[31,41,48] As can be seen from Table 2 and Figure 9, the values of N_{ss} were 4.68×10^{11} eV^{-1} cm^{-2} at 1 MHz and 3.48×10^{12} eV^{-1} cm^{-2} at 5 kHz. This result presented N_{ss} existing at the interface of the p-type Si/n-type β-$FeSi_2$ heterojunctions created by the employment of FTDCS. The existing N_{ss} behaves as the source of leakage current and a trap center for photo-generated carriers, leading to degradation of the device's performance.[24,51] According to the FESEM surface image in plain view with a magnitude of 100 k, it showed high-density gaps of crystalline domains on the surface. Therefore, the estimation error of N_{ss} should be the occurred gaps, which culminated in the non-contact area between the β-$FeSi_2$ films and Al electrodes. The real contact area is less than the nominal geometric area because the non-contact area is deducted from the nominal area.[52] Following this reasoning, the estimated N_{ss} from the nominal geometric area of 0.1 cm^2 should be slightly lower than the estimated N_{ss} from the real contact area.

Table 2. The values of various parameters for the heterojunction diodes determined from C–V and G/ω–V characteristics in f range of 5 kHz–1 MHz.

f [kHz]	V_m [V]	$(G_m/\omega)_{max}$ [F]	C_m [F]	N_{ss} [eV^{-1} cm^{-2}]	R_s [at V_m] [Ω]
5	1.45	2.75×10^{-8}	3.22×10^{-9}	3.48×10^{12}	1142.35
6	1.45	2.29×10^{-8}	3.22×10^{-9}	2.92×10^{12}	1134.29
8	1.45	1.72×10^{-8}	3.21×10^{-9}	2.23×10^{12}	1114.79
10	1.45	1.37×10^{-8}	3.21×10^{-9}	1.80×10^{12}	1101.34
20	1.45	6.99×10^{-9}	3.12×10^{-9}	1.05×10^{12}	949.34
40	1.70	3.70×10^{-9}	2.94×10^{-9}	7.54×10^{11}	659.23
60	1.95	2.72×10^{-9}	2.68×10^{-9}	6.69×10^{11}	494.98
80	2.20	2.25×10^{-9}	2.45×10^{-9}	6.15×10^{11}	403.85
100	2.40	1.95×10^{-9}	2.26×10^{-9}	5.72×10^{11}	347.60
200	3.20	1.25×10^{-9}	1.73×10^{-9}	4.56×10^{11}	217.98
400	3.95	7.57×10^{-10}	1.37×10^{-9}	4.04×10^{11}	122.92
600	4.10	5.52×10^{-10}	1.23×10^{-9}	4.11×10^{11}	80.66
800	4.15	4.40×10^{-10}	1.16×10^{-9}	4.35×10^{11}	57.14
1000	4.15	3.66×10^{-10}	1.11×10^{-9}	4.68×10^{11}	42.46

In the present work, the p-type Si/n-type β-$FeSi_2$ heterojunctions were produced via FTDCS. The occurring N_{ss} for these heterojunctions was mainly studied and estimated by the Hill-Coleman approach. In addition, the N_{ss}–f profile was provided and discussed in detail. The presence of N_{ss} at the area of heterojunction interface was confirmed, which should serve as the source of leakage current and a trap center for photo-created carriers. Additionally, it was revealed that N_{ss} increased exponentially with decreasing f. The estimated N_{ss} at f ≤100 kHz depended on f, while N_{ss} was independent of f at f >100 kHz. Furthermore, we provided the profile of the f-dependent R_s–V characteristics and described the estimated R_s values in the inversion, depletion, and accumulation

regions. In the previous research,[53] we formed the p-type Si/n-type β-$FeSi_2$ heterojunctions by RFMS.[53] The possible carrier transport mechanisms were investigated mainly by the analysis of the dark *J–V* curve. The dominant carrier transport mechanisms were a recombination process and a space-charge-limited current process at $V \leq 0.15$ V and $V > 0.15$ V, respectively.[53] Furthermore, the profile between R_s at zero bias *V* and *f* for the heterojunctions was provided. According to the explanation above, it was clear that the method of production of the heterojunctions is the difference between the two research works. Specifically, in this work, the p-type Si/n-type β-$FeSi_2$ heterojunctions were produced by FTDCS, whereas in the previous study, the p-type Si/n-type β-$FeSi_2$ heterojunctions were built via RFMS. The differences between the two production methods were explained well in the previous study.[19] For another difference, we mainly estimated the values of N_{ss} using the Hill-Coleman approach and explained the N_{ss}–*f* profile in the present work, while the previous study mainly focused on analyzing the dark *J–V* curve to provide the possible carrier transport mechanisms across the junction interface of the p-type Si/n-type β-$FeSi_2$ heterojunctions fabricated by RFMS. For the last different point, R_s as a function of *V* under various *f* was provided and discussed in the current study, while in the previous work, we estimated only R_s values at zero bias *V* under different *f* values.

4. Conclusion

In the current manuscript, the researchers created p-type Si/n-type β-$FeSi_2$ heterojunctions at a substrate temperature of 600 °C by utilization of FTDCS without a post-annealing process at high temperature. The created heterojunctions revealed a large reverse leakage current including a small response irradiated by NIR light. The *C–V–f* and *G/ω–V–f* characteristics were measured in order to estimate N_{ss} and R_s by the methods of Hill-Coleman and Nicollian-Brews, respectively. It was found that both R_s and N_{ss} values increased when *f* was decreased. The computed values of R_s at 0 V were 2.21 kΩ at 5 kHz and 13.66 Ω at 1 MHz. The values of N_{ss} were 3.48×10^{12} eV^{-1} cm^{-2} at 5 kHz and 4.68×10^{11} eV^{-1} cm^{-2} at 1 MHz. The obtained results proved the presence of N_{ss} and R_s in the created p-type Si/n-type β-$FeSi_2$ heterojunctions. These are the probable cause of the degraded heterojunction properties.

Acknowledgements

Funding of the current work was provided by the Japan International Cooperation Agency Project Office for ASEAN University Network/ Southeast Asia Engineering Education Development Network (AUN/ SEED-Net) as a project of the Collaborative Research Program for Alumni Members (CRA) (AUN/SEED-Net Project No. KMITL CRA 1701) as well as King Mongkut's Institute of Technology Ladkrabang (KMITL).

Conflict of Interest

The authors declare no conflict of interest.

Keywords

β-$FeSi_2$, FTDCS, heterojunctions, interface state density, series resistance

Received: December 10, 2017
Revised: September 5, 2018
Published online:

[1] D. B. Migas, L. Miglio, *Phys. Rev. B* **2000**, *62*, 11063.
[2] J. E. Mahan, V. L. Thanh, J. Chevrier, I. Berbezier, J. Derrien, *J. Appl. Phys.* **1993**, *74*, 1747.
[3] T. Suemasu, K. Takakura, C. Li, Y. Ozawa, Y. Kumagai, F. Hasegawa, *Thin Solid Films* **2004**, *461*, 209.
[4] H. Katsumata, Y. Makita, N. Kobayashi, H. Shibata, M. Hasegawa, I. Aksenov, S. Kimura, A. Obara, *J. Appl. Phys.* **1996**, *80*, 5955.
[5] M. Shaban, K. Nomoto, S. Izumi, T. Yoshitake, *Appl. Phys. Lett.* **2009**, *94*, 222113.
[6] M. C. Bost, J. E. Mahan, *J. Appl. Phys.* **1985**, *58*, 2696.
[7] H. Udono, I. Kikuma, *Appl. Phys. Lett.* **2004**, *85*, 1937.
[8] B. Tatar, K. Kutlu, M. Ürgen, *Thin Solid Films* **2007**, *516*, 13.
[9] N. Promros, K. Yamashita, R. Iwasaki, T. Yoshitake, *Jpn. J. Appl. Phys.* **2012**, *51*, 108006.
[10] Z. Yang, K. P. Homewood, *J. Appl. Phys.* **1996**, *79*, 4312.
[11] K. Akutsu, H. Kawakami, M. Suzuno, T. Yaguchi, K. Jiptner, J. Chen, T. Sekiguchi, T. Ootsuka, T. Suemasu, *J. Appl. Phys.* **2011**, *109*, 123502.
[12] T. Suemasu, Y. Ugajin, S. Murase, T. Sunohara, M. Suzuno, *J. Appl. Phys.* **2007**, *101*, 124506.
[13] M. Tanaka, Y. Kumagai, T. Suemasu, F. Hasegawa, *Appl. Surf. Sci.* **1997**, *117/118*, 303.
[14] T. Suemasu, Y. Negishi, K. Takakura, F. Hasegawa, T. Chikyow, *Appl. Phys. Lett.* **2001**, *79*, 1804.
[15] M. Shaban, K. Nakashima, T. Yoshitake, *Jpn. J. Appl. Phys.* **2007**, *46*, 7708.
[16] N. Promros, K. Yamashita, S. Izumi, R. Iwasaki, M. Shaban, T. Yoshitake, *Jpn. J. Appl. Phys.* **2012**, *51*, 09MF02.
[17] M. Shaban, K. Nomoto, K. Nakashima, T. Yoshitake, *Jpn. J. Appl. Phys.* **2008**, *47*, 3444.
[18] S. Izumi, M. Shaban, N. Promros, K. Nomoto, T. Yoshitake, *Appl. Phys. Lett.* **2013**, *102*, 032107.
[19] N. Promros, R. Baba, M. Takahara, T. M. Mostafa, P. Sittimart, M. Shaban, T. Yoshitake, *Jpn. J. Appl. Phys.* **2016**, *55*, 06HC03.
[20] T. Yoshitake, Y. Inokuchi, A. Yuri, K. Nagayama, *Appl. Phys. Lett.* **2006**, *88*, 182104.
[21] M. Shaban, K. Nakashima, W. Yokoyama, T. Yoshitake, *Jpn. J. Appl. Phys.* **2007**, *46*, L667.
[22] S. Nakamura, T. Aoki, T. Kittaka, R. Hakamata, H. Tabuchi, S. Kunitsugu, K. Takarabe, *Thin Solid Films* **2007**, *515*, 8205.
[23] M. Shaban, S. Izumi, K. Nomoto, T. Yoshitake, *Appl. Phys. Lett.* **2009**, *95*, 162102.
[24] P. Sittimart, A. Nopparuchikun, N. Promros, *Adv. Mater. Sci. Eng.* **2017**, *2017*, 6590606.
[25] T. Yoshitake, T. Nagamoto, K. Nagayama, *Mater. Sci. Eng.* **2000**, *B72*, 124.
[26] T. Yoshitake, T. Nagamoto, K. Nagayama, *Thin Solid Films* **2001**, *381*, 236.
[27] N. Tuğluoğlu, Ö. F. Yüksel, S. Karadeniz, H. Şafak, *Mater. Sci. Semicond. Process.* **2013**, *16*, 786.
[28] N. M. Johnson, *J. Vac. Sci. Technol.* **1982**, *21*, 303.
[29] Ç. Bilkan, A. Gümüş, Ş. Altındal, *Mater. Sci. Semicond. Process.* **2015**, *39*, 484.
[30] F. Parlaktürk, Ş. Altındal, A. Tataroğlu, M. Parlak, A. Agasiev, *Microelectron. Eng.* **2008**, *85*, 81.
[31] S. S. Fouad, G. B. Sakr, I. S. Yahia, D. M. Abdel-Basset, F. Yakuphanoglu, *Mater. Res. Bull.* **2014**, *49*, 369.

[32] S. Zeyrek, E. Acaroğlu, Ş. Altındal, S. Birdoğan, M. M. Bülbül, *Curr. Appl. Phys.* **2013**, *13*, 1225.
[33] Ş. Altındal, H. Kanbur, A. Tataroğlu, M. M. Bülbül, *Physica B* **2007**, *399*, 146.
[34] S. Monaghan, P. K. Hurley, K. Cherkaoui, M. A. Negara, A. Schenk, *Solid State Electron.* **2009**, *53*, 438.
[35] M. S. P. Reddy, J.-H. Lee, J.-S. Jang, *Synth. Met.* **2013**, *185–186*, 167.
[36] E. H. Nicollian, A. Goetzberger, *Appl. Phys. Lett.* **1965**, *7*, 216.
[37] E. H. Nicollian, A. Goetzberger, *Bell Syst. Tech. J.* **1967**, *46*, 1055.
[38] E. H. Nicollian, J. R. Brews, *MOS (Metal Oxide Semiconductor) Physics and Technology*. John Wiley & Sons, New York, New York **1982**, p. 176.
[39] M. M. Bülbül, S. Zeyrek, Ş. Altındal, H. Yuzer, *Microelectron. Eng.* **2006**, *83*, 577.
[40] I. Orak, A. Kocyigit, Ş. Altındal, *Chin. Phys. B* **2017**, *26*, 028102.
[41] B. Tataroğlu, Ş. Altındal, A. Tataroğlu, *Microelectron. Eng.* **2006**, *83*, 2021.
[42] I. Tascioğlu, W. A. Farooq, R. Turan, Ş. Altındal, F. Yakuphanoğlu, *J. Alloys Compd.* **2014**, *590*, 157.
[43] Y. Bargaoui, M. Troudi, N. Sghaier, N. Yacoubi, V. Aimez, A. Souifi, *Microelectron. Eng.* **2016**, *159*, 151.
[44] A. B. Selcuk, N. Tugluoglu, S. Karadeniz, S. B. Ocak, *Physica B* **2007**, *400*, 149.
[45] N. Konofaos, E. K. Evangelou, *Semicond. Sci. Tech.* **2003**, *18*, 56.
[46] W. A. Hill, C. C. Coleman, *Solid State Electron.* **1980**, *23*, 987.
[47] S. Zeyrek, A. Turan, M. M. Bülbül, *Chin. Phys. Lett.* **2013**, *30*, 077306.
[48] S. Karatas, A. Turut, *Microelectron. Reliab.* **2010**, *50*, 351.
[49] S. Karatas, *J. Non-Cryst. Solids* **2008**, *354*, 3606.
[50] M. M. Bülbül, S. Zeyrek, *Microelectron. Eng.* **2006**, *83*, 2522.
[51] N. Promros, K. Yamashita, C. Li, K. Kawai, M. Shaban, T. Okajima, T. Yoshitake, *Jpn. J. Appl. Phys* **2012**, *51*, 021301.
[52] Y. Xu, R. L. Jackson, D. B. Marghitu, *Int. J. Solids Struct.* **2014**, *51*, 1075.
[53] A. Nopparuchikun, N. Promros, S. Teakchaicum, P. Onsee, A. Duangrawa, P. Sittimart, *Jpn. J. Appl. Phys.* **2017**, *56*, 06HE06.